Journal of Physics: Condensed Matter

TOPICAL REVIEW

Towards electrical-current control of quantum states in spin–orbit-coupled matter

To cite this article: Gang Cao 2020 *J. Phys.: Condens. Matter* **32** 423001

IOP Publishing Journal of Physics: Condensed Matter
J. Phys.: Condens. Matter **32** (2020) 423001 (17pp) https://doi.org/10.1088/1361-648X/ab9d47

Topical Review

Towards electrical-current control of quantum states in spin–orbit-coupled matter

Gang Cao

Department of Physics, University of Colorado at Boulder, Boulder, CO 80309, United States of America

E-mail: gang.cao@colorado.edu

Received 16 April 2020, revised 14 May 2020
Accepted for publication 16 June 2020
Published 27 July 2020

Abstract

Novel materials, which often exhibit surprising or even revolutionary physical properties, are necessary for critical advances in technologies. Simultaneous control of structural and physical properties via a small electrical current is of great significance both fundamentally and technologically. Recent studies demonstrate that a combination of strong spin–orbit interactions and a distorted crystal structure in magnetic Mott insulators is sufficient to attain this long-desired goal. In this *topical review*, we highlight underlying properties of this class of materials and present two representative antiferromagnetic Mott insulators, namely, 4d-electron based Ca_2RuO_4 and 5d-electron based Sr_2IrO_4, as model systems. In essence, a small, applied electrical current engages with the lattice, critically reducing structural distortions, which in turn readily suppresses the antiferromagnetic and insulating state and subsequently results in emergent new states. While details may vary in different materials, at the heart of these phenomena are current-reduced lattice distortions, which, via spin–orbit interactions, dictate physical properties. Electrical current, which joins magnetic field, electric field, pressure, light, etc as a new external stimulus, provides a new, key dimension for materials research, and also pose a series of intriguing questions that may provide the impetus for advancing our understanding of spin–orbit-coupled matter. This *Topical Review* provides a brief introduction, a few hopefully informative examples and some general remarks. It is by no means an exhaustive report of the current state of studies on this topic.

Keywords: spin–orbit interactions, electrical-current control, spin–orbit-coupled Mott insulator, nonequilibrium state

(Some figures may appear in colour only in the online journal)

1. Overview

Electrical-current control of quantum states has been a long-sought but nearly elusive goal of science and technology. Recent studies of spin–orbit-coupled materials, particularly, 4d- and 5d-transition metal oxides [1–4], provide strong evidence that this goal may be finally within reach [5–12].

4d- and 5d-transition metal materials (4d/5d materials) feature strong spin–orbit interactions (SOI), extended d-electron orbitals, thus reduced (although still significant) on-site Coulomb interaction U, compared to 3d-transition metal materials. As shown in table 1, 4d/5d materials host a unique hierarchy of energy scales defined by comparable and competing spin–orbit and Coulomb interactions. This energy setting generates a rare, delicate interplay between the

Table 1. Comparison between compounds with 3d, 4d, and 5d electrons.[a]

Electron type	U (eV)	λ_{so} (eV)	Key interactions
3d	5–7	0.01–0.1	$U \gg \lambda_{so}$
4d	0.5–3	0.1–0.3	$U > \lambda_{so}$
5d	0.4–2	0.1–1	$U \sim \lambda_{so}$

[a] U = Coulomb interaction; λ_{SO} = SOI.

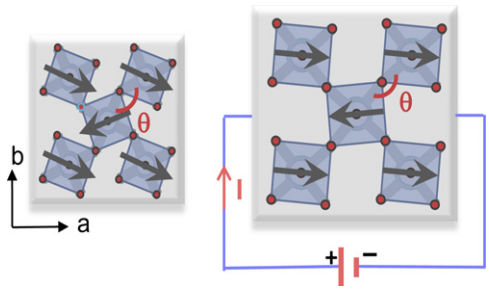

Figure 1. A schematic illustration of current-controlled structural and physical properties. The black arrows are magnetic moments strongly locked with the lattice. Applied current I engages with the lattice and relaxes lattice distortions via SOI.

fundamental interactions and leaves these materials precariously balanced on the border between different ground states, and extremely susceptible to even small, external stimuli. These stimuli strongly couple with the lattice, thus resulting in emergent novel quantum states [1, 4, 13, 14]. Electrical current, as a new external stimulus (joining magnetic field, pressure, light, etc), is surprisingly effective in coupling with the lattice, thus quantum state via SOI in certain 4d/5d materials, according to recent studies on this topic [5–12]. As schematically illustrated in figure 1, applied current relaxes and expands the lattice, thus precipitating new electronic structures or ground states. It is not surprising that current control of quantum states has rapidly become a key research topic [5–12]. Remarkably, control via application of a small current is different from control via application of static or low-frequency electric fields, such as electric-field-controlled magnetic properties in multiferroics, which is an important and yet vastly different topic that has been extensively studied over the last two decades ([15, 16], for example).

In this *tropical review*, we first present a brief survey of relevant, underlying properties of 4d/5d oxides (section 2), then focus on two representative materials recently studied (section 3) and finally conclude the article with some general remarks and an array of questions arising from the recent studies (section 4). This article provides only a glimpse of this exciting, rapidly evolving research area, and is by no means an exhaustive report of the current state of experimental studies on the topic, which is still in its infancy.

2. Fundamental characteristics of 4d- and 5d-transition metal oxides

2.1. Strong electron-lattice coupling

One key characteristic of the 4d/5d-electron transition elements is their more extended d-orbitals, compared to those of their 3d-electron counterparts. Consequently, strong p–d hybridization and electron–lattice coupling, along with the reduced intraatomic Coulomb interaction U and Hund's rule coupling J_H, are expected in these systems (see table 1). The deformations and relative orientations of corner-shared MO_6 (M = transition metal) octahedra determine the crystalline-electric-field level splitting and the electronic band structure, and hence the ground state. The physical properties of these materials are thus highly sensitive to lattice distortions and dimensionality and susceptible to external stimuli, such as application of magnetic field, pressure, light, chemical doping [1–4], or, as recently discovered, electrical current [5–12]. Some of these characteristics are well demonstrated by contrasting physical properties of the Ruddlesden–Popper (RP) series of $Ca_{n+1}Ru_nO_{3n+1}$ and $Sr_{n+1}Ru_nO_{3n+1}$ where n (=1, 2, 3, ∞) is the number of Ru–O layers per unit cell [17–30]. The ground states of this class of materials sensitively depend on the ionic radius of the alkaline earth cation, which is 1.00 Å and 1.18 Å for Ca and Sr, respectively, thus distortions and rotations/tilts of RuO_6 octahedra. As a result, the less structurally distorted $Sr_{n+1}Ru_nO_{3n+1}$ compounds are metallic and tend to be ferromagnetic (FM) (see figures 2(a) and (b)), whereas the more structurally distorted $Ca_{n+1}Ru_nO_{3n+1}$ compounds are all proximate to a metal–insulator transition and prone to antiferromagnetic (AFM) order (see figures 2(c) and (d)). Such a distinct characteristic is at the heart of numerous novel phases in the RP ruthenates uncovered via external stimuli that couple to the lattice [1].

2.2. Strong spin–orbit interactions

The inherently strong SOI are another driver of the physics of 4d/5d oxides (table 1) [1–4]. The phenomenology of the SOI and their fundamental consequences for material properties have been justifiably neglected until recently, due to the pervasive emphasis placed upon the 3d-elements in the conduct of both basic research and technical development. Nevertheless, traditional arguments would suggest that 5d-electron based oxides should be more metallic and less magnetic than oxides containing 3d, 4f or even 4d elements, because 5d-electron orbitals are more extended in space, which leads to increased electronic bandwidth. This conventional wisdom conflicts with early experimental observations in almost all existing 5d-electron based iridates such as $Sr_{n+1}Ir_nO_{3n+1}$ [31–34] and $BaIrO_3$ [35], which are conversely both AFM and insulating (see figure 3 and table 2).

It is now recognized that a critical underlying mechanism for these unanticipated states is that strong SOI that split the otherwise broad 5d-band and vigorously competes with Coulomb interactions, crystalline electric fields, and Hund's rule coupling. The so-called 'J_{eff} = 1/2' insulating state in Sr_2IrO_4 served as an early signal that the strong SOI in iridates might have unique consequences [37–39]. Since the SOI is a relativistic effect proportional to the atomic number Z or Z^2 [40, 41], it has an approximate strength of 0.4 eV in the iridates (compared to around 20 meV in 3d materials), and splits the t_{2g} 5d-bands into states with J_{eff} = 1/2 and J_{eff} = 3/2, the latter having lower energy [37, 38] (see table 1). Ir^{4+} ($5d^5$)

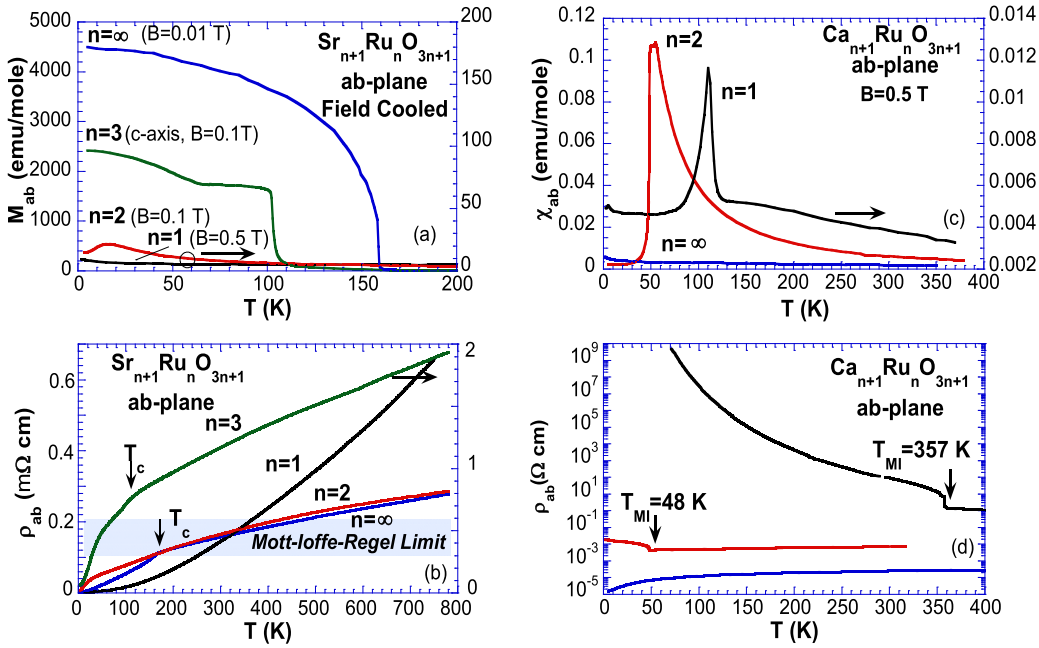

Figure 2. Basal-plane magnetic susceptibility χ, magnetization M (upper panels) and resistivity ρ (lower panels) as a function of temperature for RP series $Sr_{n+1}Ru_nO_{3n+1}$ (left column) and $Ca_{n+1}Ru_nO_{3n+1}$ (right column) with $n = 1, 2, 3$ and ∞. Note the sharp differences in the ground state between the Ca- and Sr-compounds and n-dependence of M, χ and ρ [1]. Reproduced with permission from [1].

ions provide five 5d-electrons to bonding states, four of them fill the lower $J_{\text{eff}} = 3/2$ bands, and one is left to partially fill the $J_{\text{eff}} = 1/2$ band in which the Fermi level E_F resides. The $J_{\text{eff}} = 1/2$ band is so narrow that even a reduced on-site Coulomb repulsion ($U \sim 0.5$ eV, due to the extended nature of 5d-electron orbitals) is sufficient to open a small gap Δ that stabilizes an insulating state, as shown in figure 4 [4, 37].

SOI can be modified by electronic correlations in the same way as the interatomic Coulomb interactions can be screened by itinerant electrons. It has been suggested that the effect of the Coulomb correlations can actually enhance the SOI in 4d electron systems such as Sr_2RhO_4 [42].

It is worth mentioning that Sr_2RhO_4 is similar to Sr_2RuO_4 and Sr_2IrO_4 both electronically and structurally, but its ground state is fundamentally different from those of the other two compounds. Sr_2RhO_4 hosts a Rh^{4+} ion with five 4d-electrons (compared to four 4d-electrons of the Ru^{4+} ion in Sr_2RuO_4). It shares a crystal structure remarkably similar to that of Sr_2IrO_4; in particular, the RhO_6 octahedron rotates about the c axis by 10° [43]; this value is zero for Sr_2RuO_4 and 12° for Sr_2IrO_4, as discussed below. It is argued that this octahedral rotation facilitates a correlation-induced enhancement of the SOI by about 20%, that is, the SOI increases from the bare value of 0.16 eV to 0.19 eV [42]. Despite its similarities to the insulating Sr_2IrO_4, Sr_2RhO_4 is a paramagnetic metal instead because the SOI is still not strong enough to conspire with the Coulomb interaction to open an energy gap [44], as the case in Sr_2IrO_4 discussed above and shown in figure 4. On the other hand, Sr_2RhO_4 is indeed in close proximity to an insulating state because of the octahedral rotation and the enhanced SOI—with slight Ir doping for Rh, it becomes an insulator [45]. The less robust metallic state is also because the t_{2g} bands near the Fermi surface are less dispersive in Sr_2RhO_4 than in Sr_2RuO_4, therefore more susceptible to the SOI-induced band shifts near the Fermi surface than in Sr_2RuO_4 [46]. This is in part because the $Rh^{4+}(4d^5)$ ion has five 4d electrons instead of four as in the $Ru^{4+}(4d^4)$ ion. Nevertheless, all this further highlights the very importance of both the electron–lattice coupling and SOI in 4d/5d materials.

A great deal of theoretical work has appeared in response to early experiments on iridates and motivated enormous activity in search of novel states in these materials. It is intriguing that many proposals have met limited experimental confirmation thus far. A good example is Sr_2IrO_4, an extensively studied spin–orbit-coupled material [4]. It is widely anticipated that with slight electron doping, Sr_2IrO_4 should be a novel superconductor because of its apparent similarities to those of La_2CuO_4 [47]. However, there has been no experimental confirmation of superconductivity characterized by zero resistivity and the Meissner effect, despite many years of experimental efforts. It is now recognized that the absence of the predicted superconductivity is due primarily to inherently severe structural distortions that suppress superconductivity [4, 13, 48]. A recent study reveals that the insulating state in Sr_2IrO_4 persists at megabar pressures, once again highlighting an overwhelming effect of structural distortions that prevent the expected onset of metallization, despite significant band broadening at 185 GPa [49]. On the other hand, slightly weakening the structural distortions via a newly developed field-editing technology during crystal growth nearly diminishes the insulating state in Sr_2IrO_4, according to a recent study [50]. In short, the lack of experimental confirmation of theoretical predictions of new states underscores a critical role of subtle structural distortions that dictate the low-energy Hamiltonian.

However, it is precisely this unique characteristic that permits small external stimuli, such as applied current, to readily

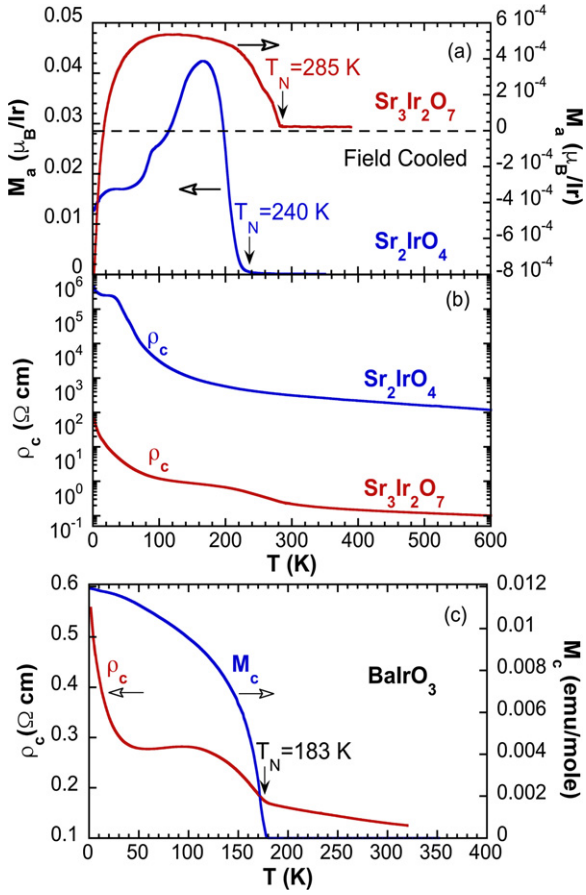

Figure 3. Temperature dependence of (a) the a-axis magnetization M_a, and (b) the resistivity ρ for Sr_2IrO_4 (blue) and $Sr_3Ir_2O_7$ (red) and (c) the c-axis resistivity ρ_c (red, left scale) and c-axis magnetization M_c (blue, right scale) for $BaIrO_3$.

Table 2. Examples of insulating and antiferromagnetic iridates.

System	Néel temperature (K)	Ground state
Sr_2IrO_4 ($n = 1$)	240	Canted AFM insulator
$Sr_3Ir_2O_7$ ($n = 2$)	285	AFM insulator
$BaIrO_3$	183	Canted AFM insulator

engage with the lattice, and, via strong magnetoelastic coupling, control magnetic and electronic states in materials hosting *a delicate interplay between* λ_{so} *and* U, as schematically illustrated in figure 5.

3. Electrical-current control of quantum states

In this section, we first review early observations of nonohmic I–V characteristics in some 4d and 5d transition metal oxides, which serve as an early sign of current-controlled behavior, and then present and discuss two model systems, namely, Sr_2IrO_4 and Ca_2RuO_4, in which application of a small current causes drastic changes in both structural and physical properties and emergent novel states otherwise unattainable.

It is important to be pointed out that Joule heating could cause spurious behavior. Therefore, extreme care must be taken to ensure that current-controlled phenomena are intrinsic. Results presented in this *Topical Review* convincingly eliminate a role of Joule heating [6, 8]. This issue is briefly discussed in sections 3.2 and 3.3 below. Nevertheless, studies of current-controlled phenomena require robust, innovative techniques that must allow adequate measurements of samples with effective control of Joule heating and temperature.

3.1. Early experimental observations of current-controlled phenomena in 4d/5d oxides

Early studies already suggested that electronic properties of certain 4d/5d oxides are sensitive to applied electrical current. In the late 1990's, it was found that $Ca_3Ru_2O_7$ [51], $BaIrO_3$ [36] and Sr_2IrO_4 [34] exhibit a 'S'-shaped, negative differential resistivity (NDR) (see figures 6–8). The NDR is in general attributed to either an 'electro-thermal' effect or a 'transferred carrier effect' in which a current promotes carriers from a high- to a low-mobility band, as in the Gunn effect. The more common form of NDR is manifest in 'N'-shaped characteristics [52–56]. Alternatively, an 'S'-shaped NDR has been observed in memory devices and a few bulk materials such as VO_2, $CuIr_2S_{4-x}Se_x$, and 1T-TaS_2 [52–58]. All of these bulk materials are characterized by a first-order metal–insulator transition without an AFM state. It is therefore peculiar for AFM Sr_2IrO_4 and $BaIrO_3$ to show the S-shaped NDR because these materials show no first-order metal–insulator transition (figure 3) [4]. Furthermore, an early study also reveals a current-induced metallic state in Sr_2IrO_4 (inset in figure 8) [34]. The current-reduced resistivity in Ca_2RuO_4 is also reported in a more recent study [59]. All results of these previous studies signaled an early sign that a combined effect of SOI and Coulomb interactions driving 4d/5d oxides may result in an unusually high susceptibility to application of electrical current. This realization helped motivate more extensive studies on this topic in recent years. Indeed, discoveries of current-induced diamagnetism in Ca_2RuO_4 [5], simultaneous current-control of structural and physical properties in Sr_2IrO_4 [6] and nonequilibrium orbital states in Ca_2RuO_4 [7–12] have been reported, respectively, since 2017. These new discoveries have arguably inaugurated the new research topic on investigations of current-controlled materials.

3.2. Model system one: spin–orbit-coupled Mott insulator Sr_2IrO_4

The AFM insulator Sr_2IrO_4 has been known for more than two decades [31–34] but it is only in recent years that the AFM insulating state is recognized as a consequence of a combined effect of strong SOI and Coulomb interactions [37] (see figure 4). As discussed above, this spin–orbit-coupled Mott insulator has an AFM transition at $T_N = 240$ K and an electronic energy gap $\Delta \leq 0.62$ eV [38, 60, 61]. It adopts a tetragonal structure with $a = b = 5.4846$ Å and $c = 25.804$ Å with space-group $I4_1/acd$ (no. 142) [62, 63], which is reduced to $I4_1/a$ (no. 88), according to more recent studies [64].

Two signature characteristics essential to current-controlled behavior are: (1) rotation of the IrO_6-octahedra about the c-axis by approximately 12°, which corresponds to a distorted

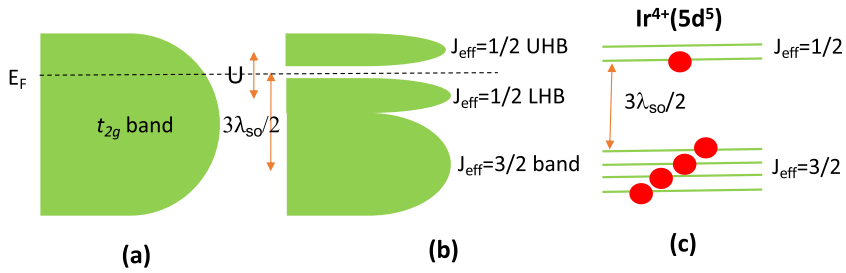

Figure 4. Band schematic: (a) the traditionally anticipated broad t_{2g} band for 5d-electrons; (b) the splitting of the t_{2g} band into $J_{eff} = 1/2$ and $J_{eff} = 3/2$ bands due to SOI; (c) $Ir^{4+}(5d^5)$ ions provide five 5d-electrons, four of them fill the lower $J_{eff} = 3/2$ bands, and one electron partially fills the $J_{eff} = 1/2$ band where the Fermi level E_F resides.

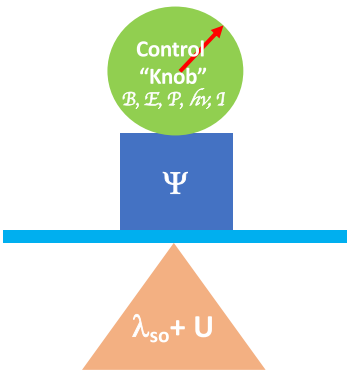

Figure 5. A schematic of the high susceptibility of a quantum state Ψ supported by λ_{so} and U to external stimuli, such as magnetic field B, electrical field E, pressure P, light $h\nu$ or electrical current I.

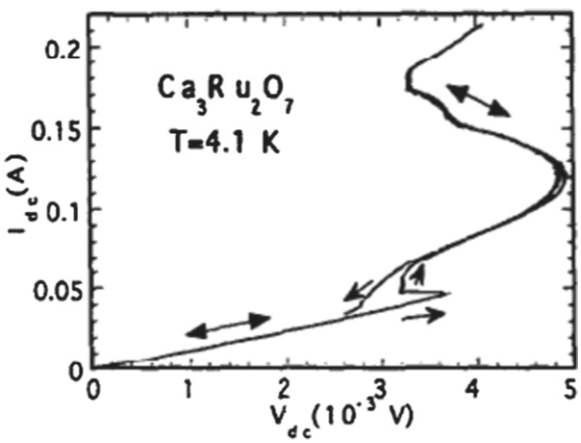

Figure 6. $Ca_3Ru_2O_7$: current–voltage characteristics: S-shaped NDR [51]. Reprinted from [51], Copyright (1998), with permission from Elsevier.

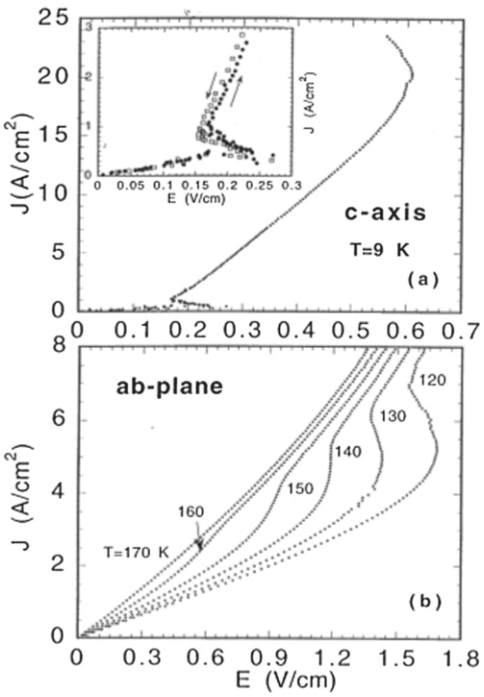

Figure 7. $BaIrO_3$: S-shaped NDR for current along (a) the c-axis and (b) the ab-plane. The inset shows details of the noisy I–V characteristics at low current and the ohmic behavior for $I = 2$ mA [36]. Reprinted from [36], Copyright (2000), with permission from Elsevier.

in-plane Ir1–O2–Ir1 bond angle θ and has a critical effect on the ground state; (2) the magnetic structure that features canted moments (0.208(3) μ_B/Ir) within the basal plane [62]. This 13(1)°-canting of the moments away from the a-axis closely tracks the staggered rotation of the IrO_6 octahedra [63, 64] (see figures 9 and 10), suggesting a strong interlocking of the magnetic moments to the lattice, which is absent in 3d oxides [65].

The relationship between the IrO_6 rotation and magnetic canting in the iridate was first discussed in reference [66], in which a theoretical model proposed a strong magnetoelastic coupling in Sr_2IrO_4, and a close association between the magnetic canting and the ratio of the lattice parameter of the c-axis to the a-axis, as a result of the strong SOI. Such a strong locking of the moment canting to the IrO_6-rotation (by 11.8(1)°) is experimentally manifest in later studies of neutron diffraction [62], x-ray resonant scattering [63] and second-harmonic generation (SHG) [64]. The SHG study also indicates that the $I41/a$ space group requires a staggering of the sign of the tetragonal distortion, which helps explain the magnetoelastic locking, as illustrated in figure 10 [64].

As demonstrated below, the strong interlocking between the lattice and magnetic moments is the key for the current control of quantum states in Sr_2IrO_4.

3.2.1. Current-controlled structural properties. Studies of crystal structures as a function of applied electrical current

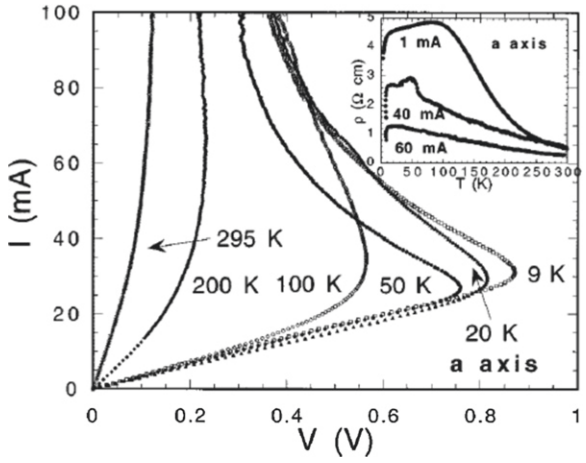

Figure 8. Sr_2IrO_4: I–V characteristics for various temperatures. Inset: ρ along the a-axis vs temperature for various currents [34]. Reprinted with permission from [34], Copyright (1998) by the American Physical Society.

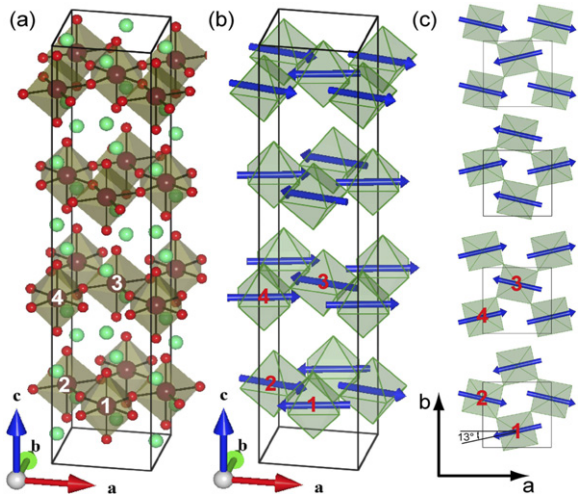

Figure 9. Sr_2IrO_4: (a) crystal structure. The IrO_6 octahedron rotates 11.8° about the c axis. The Ir atoms of the non-primitive basis are labeled 1, 2, 3, and 4. (b) The refined magnetic structure from single-crystal neutron diffraction measurements. (c) The same magnetic moment configuration projected on the basal planes [62]. Note that the magnetic canting closely tracks the IrO_6 rotation. Reprinted with permission from [62], Copyright (2013) by the American Physical Society.

have seldom or never been reported before, in part because a dependence of crystal structure on electrical current was not at all conventionally anticipated. Our study on current-controlled structural properties [6] was initiated by our early experimental observations. Among them, single-crystal Sr_2IrO_4, which was placed under a high-power microscope aided with polarizing lights, showed a slight but visible color change when current was applied to it. It is this glimmer of the unusual behavior that has eventually led to comprehensive studies of this iridate [6], and later more 4d/5d oxides [8], as functions of both electrical current and temperature.

For Sr_2IrO_4, figure 11 exhibits changes of representative Bragg peaks at $T = 200$ K with applied current within the

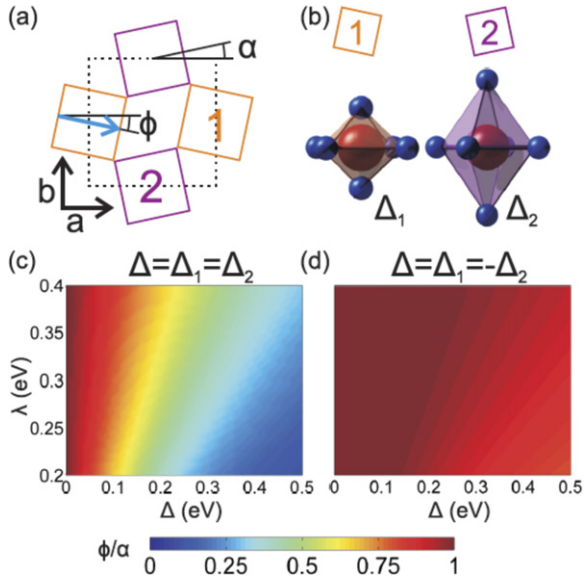

Figure 10. Sr_2IrO_4: (a) illustration of an IrO_2 plane. The oxygen octahedra rotate about the c-axis by a creating a two-sublattice structure. The magnetic moments couple to the lattice and exhibit canting angles ϕ. (b) An unequal tetragonal distortion (Δ_1 and Δ_2) on the two sublattices as required by the $I4_1/a$ space group. (c) The ratio ϕ/α as a function of both SOI λ and Δ calculated for the case of uniform and (d) staggered ($\Delta_1 = -\Delta_2$) tetragonal distortion assuming $U = 2.4$ eV, Hund's coupling $J_H = 0.3$ eV, hopping $t = 0.13$ eV, and $\alpha = 11.5°$ [64]. Reprinted with permission from [64], Copyright (2015) by the American Physical Society.

basal plane, and one of them is the peak with Miller index (0016) (figure 11(a)). A close examination of this peak reveals that both the position and intensity of the (0016) peak undergo remarkable changes at the applied current I of 105 mA (see figures 11(b) and (c)). This peak shifts up and to the right with a threefold reduction in intensity from 3260 counts at $I = 0$ mA to 999 counts at $I = 105$ mA (see figure 11(c)), suggesting significant shifts in the atomic positions. Similar changes are seen in other Bragg peaks [6].

The above results have led to more detailed investigations of the crystal structure as functions of both current and temperature, which reveal an unexpectedly large lattice expansion due to applied current. In particular, at $I = 105$ mA the a-axis elongates by nearly 1% ($\Delta a/a \equiv [a(I) - a(0)]/a(0) = 1\%$) near $T_N = 240$ K (see red curve in figure 12(a)). In contrast, the c-axis changes only very slightly ($\Delta c/c < 0.1\%$) at the same current. The contrasting response of the a- and c-axis to current I indicates an important role of the basal-plane magnetic moments (figure 9), implying the power of strong interlocking of cooperative magnetic order to the lattice (figures 9 and 10) [13, 66–68]. Indeed, the temperature dependence of $\Delta a/a$ closely tracks that of the a-axis magnetization, M_a, (black curve in figure 12(a)) whereas $\Delta c/c$ is essentially temperature independent.

This is further confirmed by a controlled study of isostructural, paramagnetic $Sr_2Ir_{0.97}Tb_{0.03}O_4$, in which a 3% substitution of Tb^{4+} for Ir^{4+} leads to a disappearance of T_N but conveniently preserves the original crystal structure and the insulating state [69] (in fact, that 3% Tb doping completely

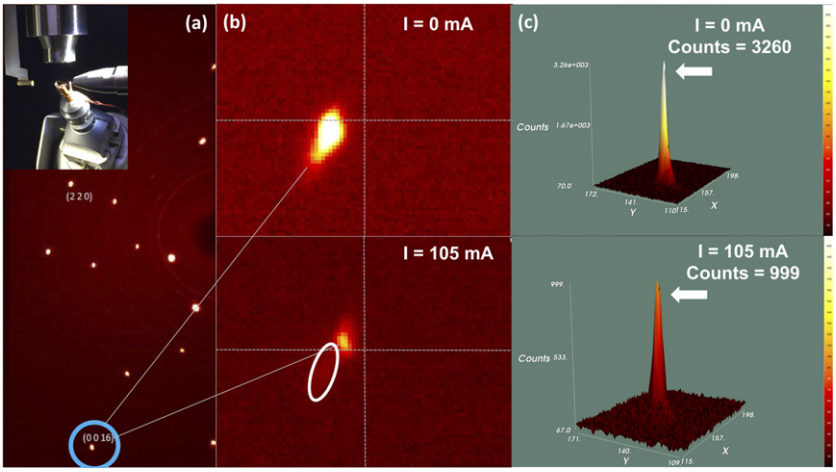

Figure 11. Sr_2IrO_4: single-crystal x-ray diffraction with current I applied within the basal plane of the crystal. (a) Representative x-ray diffraction pattern of single crystal Sr_2IrO_4. The circled Bragg peak is (0, 0, 16). Inset: sample mounting showing electrical leads and cryogenic gas feed. (b) Contrasting the (0016) peak location for $I = 0$ mA (upper panel) and $I = 105$ mA (lower panel). Note that the white oval outline marks the peak location for $I = 0$ mA for comparison. (c) The intensity of the (0016) peak is 3260 for $I = 0$ mA (upper panel) and 999 for $I = 105$ mA (lower panel) [6]. Reprinted with permission from [6], Copyright (2018) by the American Physical Society.

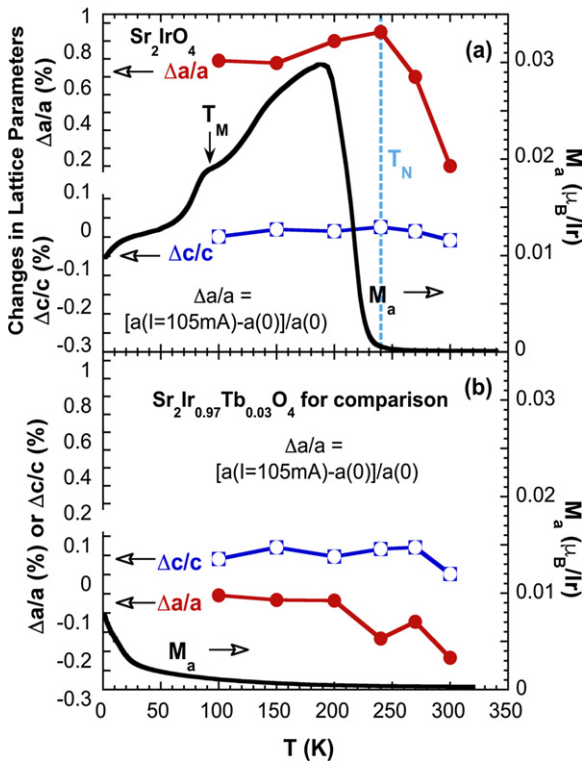

Figure 12. Current-controlled lattice change: current-controlled changes $\Delta a/a$ and $\Delta c/c$ and the a-axis magnetization M_a (right scale) for (a) AFM Sr_2IrO_4 and (b) isostructural, paramagnetic $Sr_2Ir_{0.97}Tb_{0.03}O_4$ for comparison to (a). Note that the scales for $\Delta a/a$, $\Delta c/c$ and M_a are the same in (a) and (b) for contrast and comparison [6]. Reprinted with permission from [6], Copyright (2018) by the American Physical Society.

suppresses the AFM reaffirms the high sensitivity of the magnetic properties to slight lattice changes, but an energy level mismatch for the Ir and Tb sites weakens charge carrier hopping and causes a persistent insulating state [69]). This study indicates that changes in the lattice parameters or absolute values of $\Delta a/a$ and $\Delta c/c$ at $I = 105$ mA are very small (<0.2%) and essentially temperature-dependent (figure 12(b)), the sharp contrast between figures 12(a) and (b) clearly points out a crucial role of long-range AFM in the current-induced lattice expansion [6]. Without application of current, the a axis expands by no more than ~0.1% from 90 K to 300 K due to conventional thermal expansion [6], comparable to those of many materials [70].

The contrasting lattice expansion due to application of current (~1%) and temperature (~0.1%) once again indicates an effective coupling between current and the AFM state [6].

It is also found that the lattice parameters respond differently to current I applied to the a-axis and c-axis. As shown in figure 13, the b-axis expands up to 0.8% near T_N for I applied along the a-axis (figure 13(a)) but only a half of that value for I applied along the c-axis (figure 13(b)). Moreover, the abrupt jump in $\Delta b/b$ near T_N tracks the magnetization $M(T)$, further underscoring the interlocking of the canted moments to the lattice when I is along the a axis (figure 13(a)). In contrast, $\Delta b/b$ for I along the c-axis shows no similar behavior, suggesting a much weaker coupling of current and the moments (figure 13(b)).

The anisotropic response also rules out any effect of Joule heating. Should Joule heating play an important role, then its effect would be uniform or isotropic, rather than anisotropic as seen in figure 13; additionally, the heating effect would be significantly stronger when current is applied along the c-axis because the c-axis resistivity is at least two orders of magnitude greater than the a-axis resistivity [4]. All this emphasizes that Joule heating does not play a significant role in the current-controlled phenomena in the iridate.

3.2.2. Current-controlled magnetic properties. Because of the strong coupling between the lattice and magnetic moments [62–66], it is compelling that the current-induced lattice expansion must cause changes in magnetic properties. As shown in figure 14, both the a-axis magnetic susceptibility

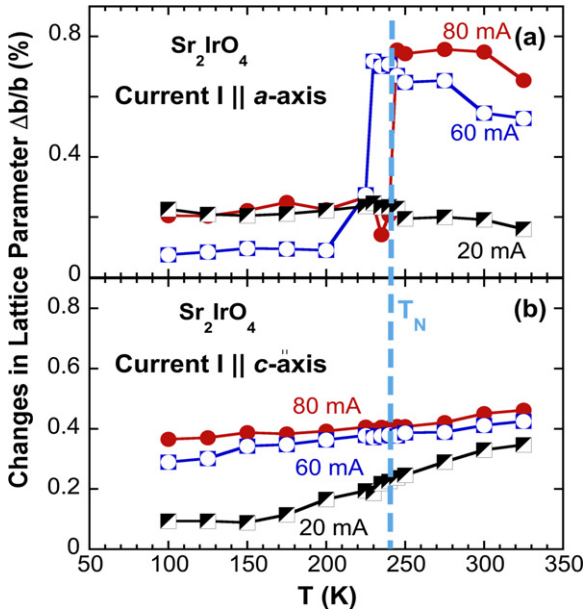

Figure 13. Sr_2IrO_4: anisotropic response of the lattice parameter b axis to current I applied along (a) the a-axis and (b) the c axis. Note that the scale for $\Delta b/b$ is the same for both (a) and (b) to facilitate comparisons. The effect of current applied along the a-axis is twice stronger than that of current applied along the c-axis. The abrupt expansion of the b-axis near T_N observed in (a) further underscores the current effect and eliminates a role of heating effect.

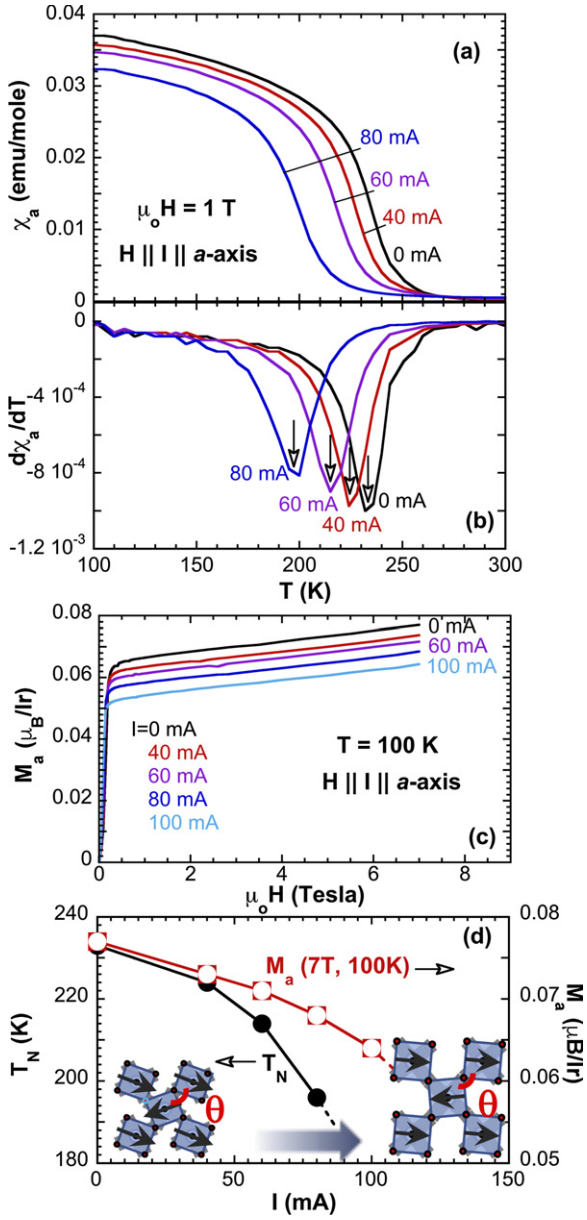

Figure 14. Sr_2IrO_4: temperature dependence of (a) a-axis magnetic susceptibility $\chi_a(T)$ at a few representative currents, and (b) $d\chi_a(T)/dT$ clarifying the decrease in T_N with I. (c) $M_a(H)$ at 100 K for a few representative currents. (d) Current dependence of T_N and M_a. Diagrams schematically illustrate the current-controlled lattice expansion, θ (red) and Ir moments (black arrows) with I [6]. Reprinted with permission from [6], Copyright (2018) by the American Physical Society.

$\chi_a(T)$ and the a-axis magnetization M_a strongly respond to the current applied along the a-axis—the AFM transition T_N is suppressed by 40 K at $I = 80$ mA (figures 14(a) and (b)) and the isothermal magnetization M_a is reduced by 16% (figure 14(c)). Magnetic canting is described by the Dzyaloshinsky–Moriya interaction, i.e., $\mathbf{D}\bullet(\mathbf{S_i}\mathrm{x}\mathbf{S_j})$; the vector $\mathbf{D}$, which measures distortions, approaches zero when the neighboring spins $\mathbf{S_i}$ and $\mathbf{S_j}$ become collinearly aligned. The magnetic changes presented in figure 14 are therefore understandable because the applied current relaxes the Ir–O–Ir bond angle θ, thus weakens magnetic canting and the overall AFM state, as schematically illustrated in figure 14(d).

3.2.3. Current-controlled transport properties and non-ohmic I–V characteristics. The current-induced lattice expansion also enhances electron mobility in general and precipitates an unusual quantum switching effect in particular. As shown in figures 15(a)–(c), a linear I–V response during an initial current increase is followed by a sharp threshold voltage V_{th}, indicating a switching point where V abruptly drops with increasing I. This switching point is followed by another broad turning point that emerges at a higher current. A strong anisotropy in the IV-characteristics for the a-axis (figure 15(a)) and c-axis (figure 15(b)) is illustrated in figure 15(c) [6].

Interestingly, the threshold voltage V_{th} as a function of temperature shows a distinct slope change near a magnetic anomaly $T_M \approx 100$ K [13] (see figure 16). Early studies [13, 71, 72] have demonstrated that the magnetization M_a undergoes additional anomalies at $T_M \approx 100$ K and 25 K (figure 16, black curve, right scale), due chiefly to moment reorientations [72]. This magnetic reorientation separates the different regimes of I–V behavior below and above $T_M \approx 100$ K (figure 16). The concurrent changes in both V_{th} and M_a strongly indicates a close correlation between the I–V characteristics and magnetic state, and, more generally, a mechanism that is fundamentally different from that operating in other materials [53].

Furthermore, an emergent metallic state similar to that previously observed (inset in figure 8) also occurs at 20 mA [6].

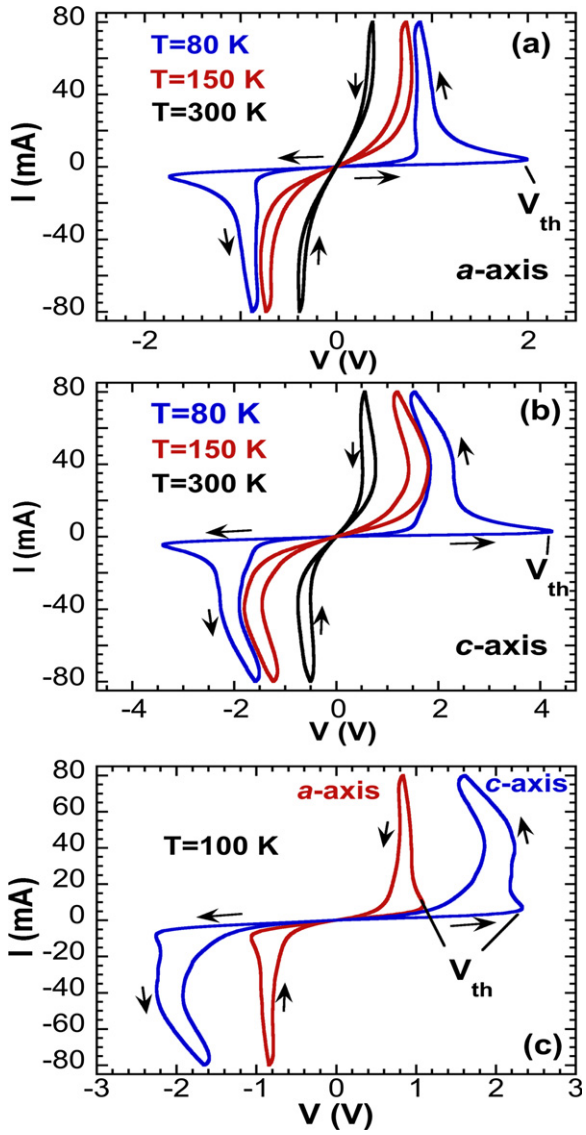

Figure 15. Sr_2IrO_4: I–V curves at representative temperatures for: (a) current applied along the a-axis, (b) along the c-axis, (c) both the a- and c-axis at $T = 100$ K. Arrows show the evolution of the current sweeps in (a) to (c) [6]. Reprinted with permission from [6], Copyright (2018) by the American Physical Society.

Nevertheless, the current-controlled a-axis expansion $\Delta a/a$ [upper horizontal axis in figure 17(a)] closely tracks the I–V curves with non-linear changes at two critical currents I_{C1} (=10 mA) and I_{C2} (=45 mA), respectively [6]. The slope changes in $\Delta a/a$ indicate successively more rapid expansions of the a-axis at I_{C1} and I_{C2}, and each of them is accompanied by a more significant increase in the Ir–O–Ir bond angle θ, which in turn improves electron hopping (figure 17(b)). The a-axis expansion $\Delta a/a$ seems to saturate as the current further increases above $I_{C2} = 45$ mA, suggesting that the lattice parameters cannot further expand at $I > I_{C2}$. This explains why a magnetic field H reduces V considerably only between I_{C1} and I_{C2} but shows no visible effect above I_{C2} (green curve in figure 17(a)), where the saturation of $\Delta a/a$ corresponds to θ approaching 180°, which prevents further increases.

The correlation between the a-axis expansion (figure 12), the magnetic canting (figures 9 and 16) and the I–V curves

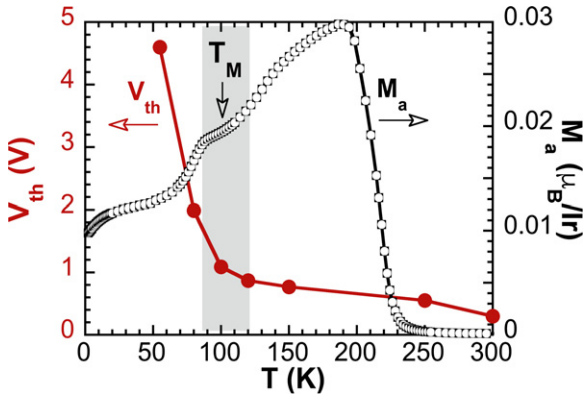

Figure 16. Sr_2IrO_4: correlation between the switching effect and magnetization temperature dependence of the threshold voltage V_{th} for the a-axis (red) and a-axis magnetization $M_a(T)$ (black). Note the slope change of V_{th} near T_M.

(figure 15) highlights a crucial role of the current-controlled basal-plane expansion that dictates the quantum states. In essence, this is because the IrO_6-octahedra and the canted moment are locked together, thus rigidly rotate together (figures 9 and 10) due to strong SOI; applied electrical current effectively engages with the lattice and expands the basal plane by increasing θ, which in turn reduces the magnetic canting and the AFM transition T_N and enhances the electron mobility, as illustrated in figure 17.

It is important to be pointed out that current-controlled phenomena are essentially absent in the spin–orbit-coupled $Sr_3Ir_2O_7$ (figure 3) [35], a sister compound of Sr_2IrO_4, in part because of its collinear magnetic structure, which is discussed in section 4. Recent studies reveal that current-controlled phenomena exist in a range of Mott systems having magnetic and/or structural distortions.

3.3. Model system two: structurally-driven Mott insulator Ca_2RuO_4

Structurally-driven Mott insulator Ca_2RuO_4 [24, 73] is another model system [5, 7, 8]. As discussed in section 2.1, this material exhibits a metal–insulator transition at $T_{MI} = 357$ K driven by a violent structural transition [25]. This transition is accompanied by a severe rotation and tilting of RuO_6 octahedra, resulting in a considerably enhanced orthorhombicity below T_{MI}, and lifting the t_{2g} orbital (d_{xy}, d_{yz}, d_{zx}) degeneracy [25, 26, 74–83]. An AFM state is only stabilized at a much lower temperature, $T_N = 110$ K [24, 73] by a further rotation and tilting of RuO_6 octahedra. It is now well-recognized that physical properties are dictated by the structural distortions and the populations of t_{2g} orbitals, particularly, the d_{xy} orbital [26, 70, 73–86].

We choose 3% Mn doped Ca_2RuO_4 or $Ca_2Ru_{0.97}Mn_{0.03}O_4$ for this investigation because the dilute Mn doping weakens the violent first-order structural phase transition at 357 K but preserves the underlying structural and physical properties of Ca_2RuO_4. This way, the single crystals are more robust to sustain thermal cycling necessary for thorough measurements [70, 86]. Note that a key effect of the slight Mn or other 3d ion doping on Ca_2RuO_4 is the weakening of the

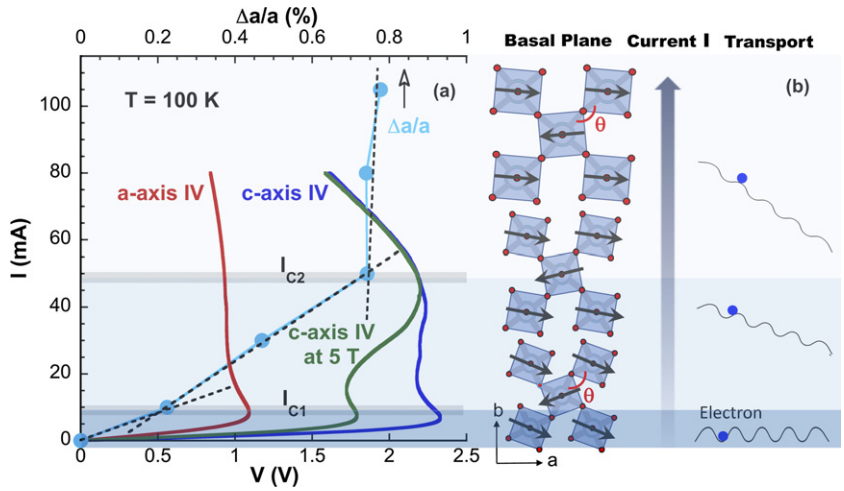

Figure 17. Sr_2IrO_4: (a) I–V curves (red, blue, green) for a- and c-axis at $T = 100$ K and applied magnetic field of 0 or 5 T along the c-axis. Light blue data (upper horizontal axis) show current-controlled a-axis expansion $\Delta a/a$ at $T = 100$ K. Dashed lines are guides to the eye. Note slope changes of $\Delta a/a$ occur at the two turning points of the I–V curves at I_{C1} and I_{C2}, respectively. (b) Diagrams (not to scale) illustrate the expanding lattice, increasing Ir1–O2–Ir1 bond angle θ (red) and decreasing magnetic canting (black arrows) with increasing I. The reduced lattice distortions lead to enhanced electron mobility (see schematic) [6]. Reprinted with permission from [6], Copyright (2018) by the American Physical Society.

severe orthorhombicity while preserving the low-temperature orthorhombic symmetry (*Pbca*). Since the doping level is very low, the carrier concentration remains essentially unchanged [70, 86].

As discussed in section 3.2, the key element here is a novel coupling between small applied electrical current and the lattice that, in an extraordinary fashion, reduces the orthorhombic distortion, the octahedral rotation and tilt. These lattice changes in turn readily suppress the native AFM state and subsequently induce a nonequilibrium orbital state. A phase diagram generated based on the data illustrates a narrow critical regime near a small current density of 0.15 A cm^{-2} that separates the native, diminishing AFM state and the emergent, nonequilibrium orbital state. It is particularly significant that a direct correlation between the current-reduced orthorhombicity and electrical resistivity is established via simultaneous measurements of both neutron diffraction and electrical resistivity. Notably, no current-induced diamagnetism, which is reported to exist in Ca_2RuO_4 [5], is observed in both doped and undoped Ca_2RuO_4 in this study.

In the following, we first discuss current-induced changes in the magnetization, electrical resistivity and then the lattice modifications and the correlation between them.

3.3.1. Current-controlled magnetization and electrical resistivity. As shown in figures 18(a) and (b), the a- and b-axis magnetization, M_a and M_b, changes drastically with electrical current applied along the b axis. The AFM transition T_N drops rapidly from 125 K at current density $J = 0$ A cm^{-2} to 29 K at $J = 0.15$ A cm^{-2} in M_b, and completely disappears at $J > J_C \sim 0.15$ A cm^{-2} [8] (Note that 0.15 A cm^{-2} is a remarkably small current density!) The vanishing AFM state is accompanied by a drastic decrease in the b-axis resistivity, ρ_b, by up to four orders of magnitude (figure 18(c)). Note that the resistivity and magnetization are simultaneously measured.

A few points are particularly remarkable and are discussed in the following sections.

3.3.2. Emergent nonequilibrium orbital state

Upon the vanishing of the AFM transition T_N, a distinct phase characterized by T_O emerges below 80 K (see figure 19). The phase transition T_O rises initially, peaks at $J = 0.28$ A cm^{-2} before decreasing with increasing J (figure 19(a)). The b-axis resistivity ρ_b intimately tracks the magnetization M_a (figure 19(b)). The *concurrent change* in both ρ_b and M_a at T_O indicates a strong correlation between the transport and magnetic properties in the emergent state, which sharply contrasts the native state in which T_N happens nearly 250 K below T_{MI} [24, 25, 74], implying that the nature of the current-induced state is distinctly different from that of the native state. This is consistent with the fact that it emerges only when the equilibrium AFM state completely vanishes.

Above To, the magnetization shows a history-dependence (not shown), which is most likely associated with a metastable state. It is already established that the current-reduced structural distortions effectively diminish the AFM at $J \geq 0.15$ A cm^{-2} (figure 18), thus favoring a competing FM state [76, 79]. Further increasing J inevitably enhances the competition between the FM and AFM interactions but in a metastable manner, leading to the history-dependent behavior. The neutron diffraction rules out any current-induced inhomogeneous effect [8].

3.3.3. No diamagnetism discerned

It is stressed that the emergent state at $J > J_C$ is also observed in undoped Ca_2RuO (figure 20(a)), and 9% Mn doped Ca_2RuO_4 (figure 20(b)). This indicates that the new state is a robust response of Ca_2RuO_4 to applied current, independent of Mn doping. Importantly, the data in figures 19

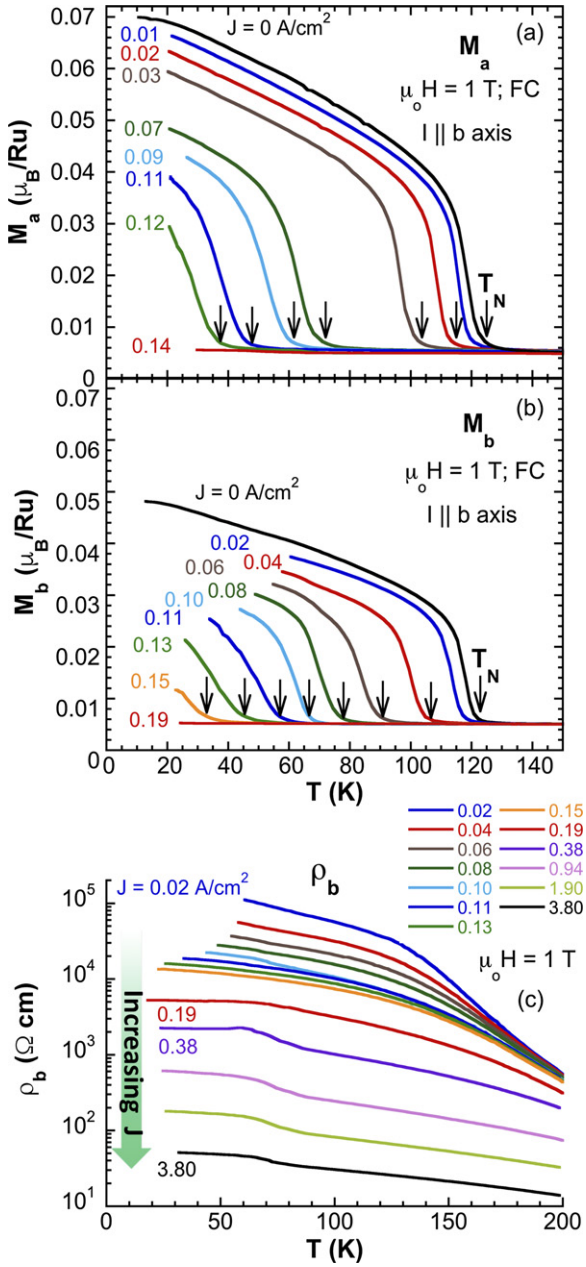

Figure 18. Current-driven magnetic and transport properties of $Ca_2Ru_{0.97}Mn_{0.03}O_4$: the temperature dependence at various J applied along the b axis of (a) the a-axis magnetization M_a, (b) the b-axis magnetization M_b and (c) the b-axis resistivity ρ_b. The magnetic field is at 1 T [8]. Reprinted with permission from [8], Copyright (2019) by the American Physical Society.

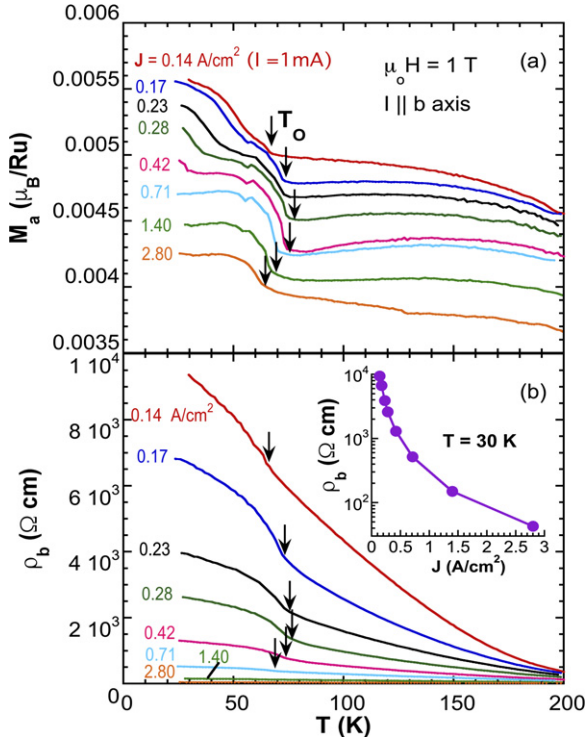

Figure 19. Current-induced ordered state at $J \geqq 0.14$ A cm^{-2}: the temperature dependence at various J applied along the b axis of (a) M_a at 1 T and (b) ρ_b for $Ca_2Ru_{0.97}Mn_{0.03}O_4$; inset: ρ_b at 30 K as a function of J [8]. Reprinted with permission from [8], Copyright (2019) by the American Physical Society.

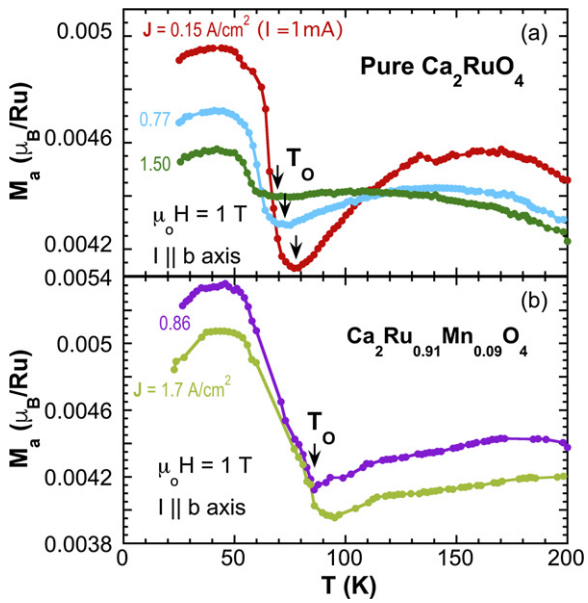

Figure 20. Pure Ca_2RuO_4 and $Ca_2Ru_{0.91}Mn_{0.09}O_4$ for comparison: the a-axis magnetization M_a at 1 T at a few representative J for (a) pure Ca_2RuO_4 and (b) $Ca_2Ru_{0.91}Mn_{0.09}O_4$ [8]. Reprinted with permission from [8], Copyright (2019) by the American Physical Society.

and 20 show no sign of the diamagnetism prominently reported in Science 358, 1084 (2017) or reference [5]. A controlled study on other magnetic materials [8] further buttresses the conclusion: no current-induced diamagnetism in both undoped and doped Ca_2RuO_4 [8]. Such a major discrepancy between results in references [5, 8] deserves more investigations.

3.3.4. Quantum switching effect

As in Sr_2IrO_4, a sharp, unusual switching effect is also a pronounced feature in Ca_2RuO_4, as shown in figure 21 (note that the data is taken from $Ca_2Ru_{0.97}Mn_{0.03}O_4$ because it can sustain more thermal cycles than undoped Ca_2RuO_4). The mechanism of the switching effect is likely similar to that operating

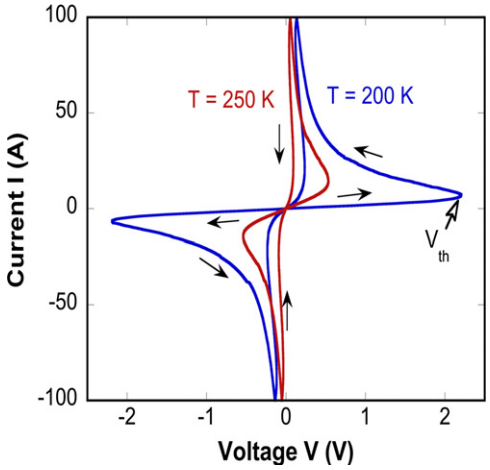

Figure 21. I–V characteristics for $Ca_2Ru_{0.97}Mn_{0.03}O_4$ at $T = 200$ and 250 K. Note that the I–V curves are taken above T_O (~80 K).

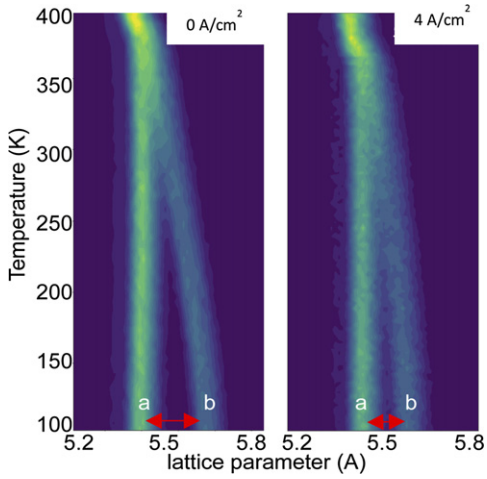

Figure 22. The neutron diffraction and current-reduced orthorhombicity in $Ca_2Ru_{0.97}Mn_{0.03}O_4$: two representative contour plots for the temperature dependence of the lattice parameters a, and b axis at current density $J = 0$ and 4 A cm^{-2} applied in the basal plane. Note the diminishing orthorhombicity with increasing J marked by the red arrows [8]. Reprinted with permission from [8], Copyright (2019) by the American Physical Society.

in Sr_2IrO_4, i.e., the current-induced lattice expansion drives the I–V characteristics, as discussed in section 3.2.

3.3.5. Current-controlled structural properties. The structural properties as functions of applied current and temperature are thoroughly studied via neutron diffraction. A major effect is the diminishing orthorhombicity with increasing J, as shown in figure 22. Indeed, the orthorhombicity, defined by $(b - a)/[(a + b)/2]$, readily reduces with increasing J—from 4.4% at $J = 0$ A cm^{-2} to 1.2% at $J = 30$ A cm^{-2} (figures 23(a) and (b)). At the same time, the c axis expands by up to 2.4% at $J = 30$ A cm^{-2} (figure 23(c)). It is also crucial that the bond angle Ru–O–Ru, which defines the rotation of RuO_6 octahedra, increases by up to two degrees at $J = 18$ A cm^{-2}, giving rise to much less distorted RuO_6 octahedra (figure 23(d)). Furthermore, the bond angle O–Ru–O decreases from 91° to

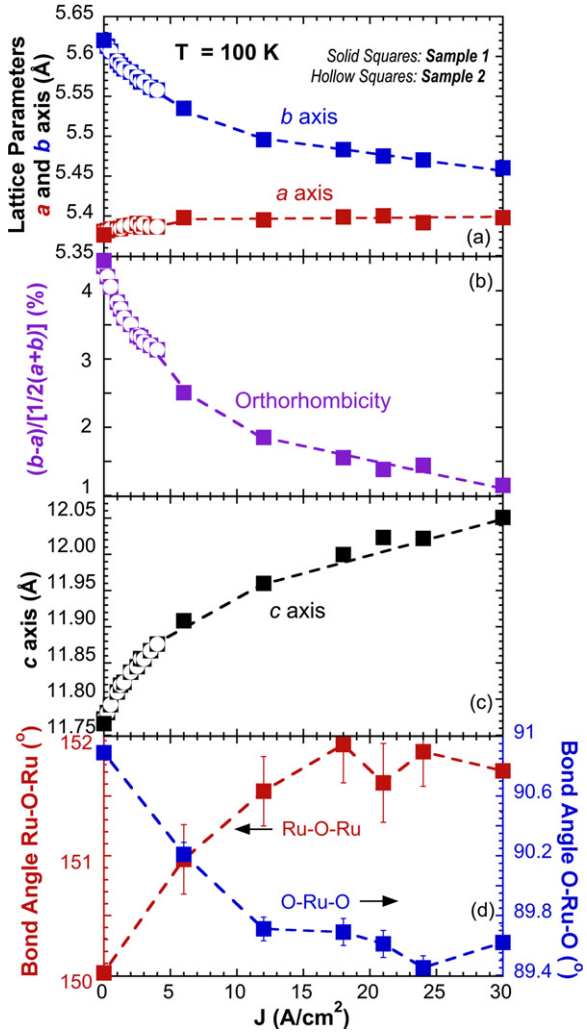

Figure 23. The neutron diffraction and current-driven lattice changes in $Ca_2Ru_{0.97}Mn_{0.03}O_4$ The current density J dependence at 100 K of (a) the a and b axis, (b) the orthorhombicity, (c) the c axis and (d) the bond angles Ru–O–Ru (red, left scale) and O–Ru–O (blue, right scale) [8]. Reprinted with permission from [8], Copyright (2019) by the American Physical Society.

90.2° at $J = 5$ A cm^{-2}, close to the ideal O–Ru–O bond angle of 90° (figure 23(d)). The significantly relaxed crystal structure explains the transport and magnetic data in figures 18–21. This strong, direct association is further illustrated below.

3.3.6. Correlations between current-controlled structural and physical properties. The simultaneous measurements of neutron diffraction and electrical resistivity highlight a direct link between the current-reduced orthorhombicity and resistivity (see figure 24). The orthorhombicity as functions of temperature and current density ranging from 0 to 4 A cm^{-2} in figure 24(a) shows that the orthorhombic distortion rapidly reduces with current density J (<1 A cm^{-2}). At the same time, the resistivity almost perfectly tracks the orthorhombicity, as shown in figure 24(b): the contour-plot comparison of figures 24(a) and (b) compellingly establishes an explicit correlation between the current-driven lattice and transport properties. Indeed, the improved structure significantly improves

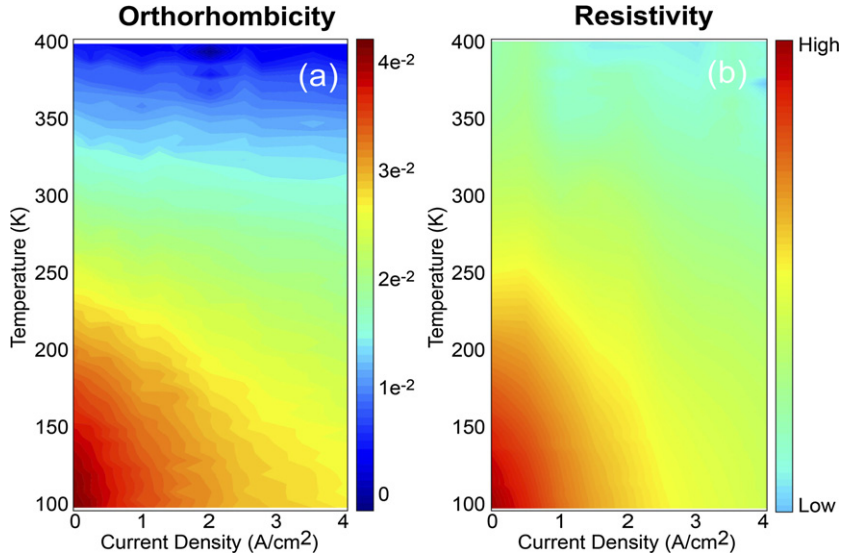

Figure 24. Direct correlation between the orthorhombicity and the electrical resistivity of $Ca_2Ru_{0.97}Mn_{0.03}O_4$: the temperature–current-density contour plots for (a) the orthorhombicity and (b) electrical resistivity [8]. Reprinted with permission from [8], Copyright (2019) by the American Physical Society.

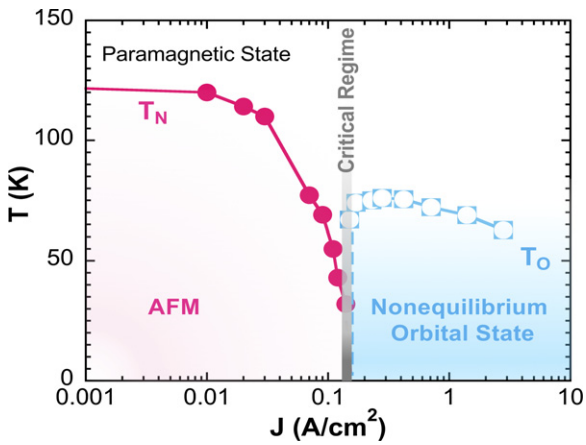

Figure 25. The T–J phase diagram illustrates that the applied current drives the system from the native AFM state (purple) through the critical regime near 0.15 A cm^{-2} (gray) to the current-induced, nonequilibrium orbital state (blue) [8]. Reprinted with permission from [8], Copyright (2019) by the American Physical Society.

the t_{2g} orbital occupancies for better electron hopping, as also evidenced in figures 18 and 19.

It also deserves to be stressed that the structural transition T_{MI}, which is defined by the blue area in figure 24(a), hardly shifts with the current density J. This is also true for the data in figure 22. These data along with the data for Sr_2IrO_4 discussed in section 3.2 further confirm that Joule heating effect is inconsequential in these studies [6, 8].

3.3.7. Phase diagram and nonequilibrium orbital state. A temperature–current-density phase diagram generated based on the data presented above summarizes the current-controlled phenomena in Ca_2RuO_4: by reducing the structural distortions and changing t_{2g} orbital occupancies, the applied current effectively destabilizes the insulating and AFM state and, at a narrow critical regime of current density J_C, precipitates the nonequilibrium orbital state, as shown in figure 25.

In ambient conditions, the tetravalent Ru^{4+} ion with four 4d electrons ion provides 2 holes in the t_{2g} orbitals (with empty e_g orbitals). A 1/2-hole is transferred to the oxygen [1], and the remaining 3/2 hole is equally split in a 1:1 ratio between the d_{xy} orbital and the manifold of d_{xz}/d_{xz} orbitals at high temperatures or in the metallic state at $T > T_{MI}$. At $T < T_{MI}$, the first-order transition $T_{MI} = 357$ K enhances the orthorhombicity and other distortions including the rotation, tilting and flattening of octahedron RuO_6. These changes facilitate a transfer of more holes from d_{xy} to d_{xz}/d_{yz}, or a 1:2 ratio of hole occupancies in d_{xy} vs d_{xz}/d_{yz} [1]. The insulating state below T_{MI} thus has each orbital at exactly 3/4 electron filling. This contrasts the metallic state above T_{MI} which has a nearly half-filled d_{xy} orbital and unequal filling, with a nearly filled d_{xz}/d_{yz} manifold.

The half-filled orbital d_{xy} is the key to the metallic state. The applied current helps stabilize the existence of the half-filled orbital d_{xy} as temperature decreases by minimizing structural distortions (orthorhombicity, octahedral rotation and tilt). These current-induced lattice changes also explain the vanishing native AFM state with increasing J because it delicately depends on a combination of rotation, tilt and flattening of RuO_6 octahedra [76–83], all of which are significantly weakened by applied current, as shown in figures 22–24.

While the understanding of the nonequilibrium orbital state at $J > J_C$ (figure 25) is yet to be fully established, it is clear that at the heart of the current-controlled phenomena are the critical lattice modifications via current-driven nonequilibrium orbital populations.

4. Challenges and outlook

Mounting experimental evidence indicates that current controlled phenomena are widespread and present in a range of

high-Z materials including both oxides and chalcogenides having an (anti)ferromagnetic and insulating state [87]. Recent studies point out a few empirical trends.

First of all, current-controlled materials must have comparable SOI and U and a ground state that is both (anti)ferromagnetic and insulating. It is apparent that 4d/5d materials provide an energy setting more desirable for current control of quantum states because the 4d/5d electronic wave functions are more extended, the d-band width is wider, and U and J_H are smaller than those in the 3d transition metal oxides (table 1), as discussed in section 2. In these materials, the insulating and magnetic ground state is not enabled by large U but rather driven by subtle interactions which are assisted by SOI; thus, a small external stimulus such as electrical current could be sufficient to produce a large response, leading to phase transitions, as illustrated in the cases of Sr_2IrO_4 and Ca_2RuO_4.

Secondly, an effective current control of quantum states also requires the presence of a distorted crystal structure, oftentimes, canted moments and a strong magnetoelastic coupling. A distorted structure such as rotations and/or tilts of octahedra MO_6 generates room for applied current to relax correlated octahedral rotations and/or tilts and magnetic structures via a strong magnetoelastic coupling that locks magnetic moments with the lattice through SOI [58–60]. This point is demonstrated in $Sr_3Ir_2O_7$ [35] in which current-controlled behavior is essentially absent. This double-layered iridate is a sister compound of Sr_2IrO_4 and an AFM insulator with $T_N = 285$ K and equally strong SOI (figures 3(a) and (b)) [4, 35]. However, the magnetic moments in $Sr_3Ir_2O_7$ are collinearly aligned along the c axis [88, 89] rather than canted within the basal plane where the octahedral rotation occurs, contrasting with that of Sr_2IrO_4. As a result, applied current cannot exert a sufficient effect because the collinearly aligned magnetic moments along the c axis is not strongly coupled with the IrO_6 rotation. Therefore, $Sr_3Ir_2O_7$ hardly shows current-controlled behavior observed in Sr_2IrO_4.

In short, the search of current-controlled materials should focus on AFM Mott insulators with strong structural and/or magnetic distortions in high-Z materials where the role of SOI is significant and electron orbitals are extended—SOI lock magnetic moments to the lattice and the extended orbitals facilitate a strong coupling of current and electron orbitals. An effective current-control of quantum states is not anticipated in low-Z materials such as 3d materials because of the lack of the key elements.

While current-controlled phenomena and materials pose tantalizing prospects for unique functional materials and devices, a better understanding of them must be established. Clearly, theoretical efforts are urgently needed to help gain more insights into the physics of the nonequilibrium phenomena in correlated and spin–orbit-coupled materials.

Nevertheless, the empirical trends observed in recent years help pose a series of intriguing questions that may provide the impetus for advancing our understanding of this class of materials:

- Current-driven phenomena are essentially nonequilibrium phenomena, which are both exciting and intellectually challenging; how can we more comprehensively tackle the challenge both theoretically and experimentally?
- In particular, how can we adequately describe the coupling of current and the lattice and/or magnetic moments in this class of materials? This is among key issues for this research topic and needs to be addressed urgently.
- Can an applied current increase the mixing of the $J_{eff} = 1/2$ and $J_{eff} = 3/2$ states and be responsible for the dramatic current-induced changes in the iridates?
- While the non-ohmic I–V characteristics are closely associated with the current-induced lattice expansion experimentally, how can we adequately describe changes in band structures fundamentally responsible for them?
- How can we more effectively current-control structural, magnetic and transport properties?
- More generally, can we establish a set of criteria to identify and improve these materials?
- What are potential applications of this class of materials?
- What unique devices can we propose or develop using the novel current-controlled properties?

It is clear that current control of quantum states opens new avenues for better understanding the fundamental physics of spin–orbit-coupled matter. Equally importantly, it also provides a new paradigm for the development of an entire class of current-controlled materials to underpin functional devices otherwise unavailable.

Endnote: Upon the completion of this *Topical Review*, a newly posted arXiv manuscript, which is authored by the same research group that reported the diamagnetism in *Science* **358** 1084 (2017) or [5], attributes the reported diamagnetism to *spurious behavior* rather than intrinsic response to the applied current [90]. More recently, the authors of *Science* **358** 1084 (2017) and *Physical Review Letters* **122** 196602 (2019) (on diamagnetism in $Ca_3(Ru_{1-x}Ti_x)_2O_7$) retract the two papers [91, 92].

Acknowledgments

The author is indebted to Mr Hengdi Zhao, Dr Bing Hu, Dr Feng Ye and Dr Lance DeLong for useful discussions when writing this *Topical Review*. This work is supported by the US National Science Foundation via Grant DMR-1903888.

ORCID iDs

Gang Cao https://orcid.org/0000-0001-9779-430X

References

[1] Cao G and DeLong L 2013 *Frontiers of 4d- and 5d-Transition Metal Oxides* (Singapore: World Scientific)
[2] Witczak-Krempa W, Chen G, Kim Y B and Balents L 2014 Correlated quantum phenomena in the strong spin–orbit regime *Annu. Rev. Condens. Matter Phys.* **5** 57

[3] Rau J G, Lee E K H and Kee H Y 2016 Spin–orbit physics giving rise to novel phases in correlated systems: iridates and related materials *Annu. Rev. Condens. Matter Phys.* **7** 195

[4] Cao G and Schlottmann P 2018 The challenge of spin–orbit-tuned ground states in iridates: a key issues review *Rep. Prog. Phys.* **81** 042502

[5] Sow C, Yonezawa S, Kitamura S, Oka T, Kuroki K, Nakamura F and Maeno Y 2017 Current-induced strong diamagnetism in the Mott insulator Ca_2RuO_4 *Science* **358** 1084–7

[6] Cao G, Terzic J, Zhao H D, Zheng H, De Long L E and Riseborough P S 2018 Control of structural and physical properties via strong spin–orbit interactions in Sr_2IrO_4 *Electr. Phys. Rev. Lett.* **120** 017201

[7] Bertinshaw J *et al* 2019 Unique crystal structure of Ca_2RuO_4 in the current stabilized semimetallic state *Phys. Rev. Lett.* **123** 137204

[8] Zhao H, Hu B, Ye F, Hoffmann C, Kimchi I and Cao G 2019 Nonequilibrium orbital transitions via applied electrical current in calcium ruthenates *Phys. Rev.* B **100** 241104(R)

[9] Zhang J *et al* 2019 Nano-resolved current-induced insulator-metal transition in the Mott insulator Ca_2RuO_4 *Phys. Rev.* X **9** 011032

[10] Bertinshaw J *et al* 2019 Unique crystal structure of Ca_2RuO_4 in the current stabilized semimetallic state *Phys. Rev. Lett.* **123** 137204

[11] Cirillo C, Granata V, Avallone G, Fittipaldi R, Attanasio C, Avella A and Vecchione A 2019 Emergence of a metallic metastable phase induced by electrical current in Ca_2RuO_4 *Phys. Rev.* B **100** 235142

[12] Okazaki R, Kobayashi K, Kumai R, Nakao H, Murakami Y, Nakamura F, Taniguchi H and Terasaki I 2020 Current-induced giant lattice deformation in the Mott insulator Ca_2RuO_4 *J. Phys. Soc. Japan* **89** 044710

[13] Ge M, Qi T F, Korneta O B, De Long L E, Schlottmann P and Cao G 2011 Lattice-driven magnetoresistivity and metal–insulator transition in single-layered iridates *Phys. Rev.* B **84** 100402

[14] Zheng H, Song W H, Terzic J, Zhao H D, Zhang Y, Ni Y F, DeLong L E, Schlottmann P and Cao G 2018 Observation of a pressure-induced transition from interlayer ferromagnetism to intralayer antiferromagnetism in $Sr_4Ru_3O_{10}$ *Phys. Rev.* B **98** 064418

[15] Kimura T, Goto T, Shintani H, Ishizaka K, Arima T and Tokura Y 2003 Magnetic control of ferroelectric polarization *Nature* **426** 55

[16] Tokura Y, Seki S and Nagaosa N 2014 Multiferroics of spin origin *Rep. Prog. Phys.* **77** 076501

[17] Cao G, McCall S, Crow J E and Guertin R P 1997 Observation of a metallic antiferromagnetic phase and metal to nonmetal transition in $Ca_3Ru_2O_7$ *Phys. Rev. Lett.* **78** 1751

[18] Allen P, Berger H, Chauvet O, Forro L, Jarlborg T, Junod A, Revaz B and Santi G 1996 Transport properties, thermodynamic properties, and electronic structure of $SrRuO_3$ *Phys. Rev.* B **53** 4393

[19] Cao G, McCall S, Shepard M, Crow J E and Guertin R P 1997 Thermal, magnetic, and transport properties of single crystal $Sr_{1-x}Ca_xRuO_3$ ($0 < x < 1.0$) *Phys. Rev.* B **56**321

[20] Mazin I I and Singh D J 1997 Electronic structure and magnetism in Ru-based perovskites *Phys. Rev.* B **56** 2556

[21] Klein L, Dodge J S, Ahn C H, Snyder G J, Geballe T H, Beasley M R and Kapitulnik A 1996 Anomalous spin scattering effects in the badly metallic itinerant ferromagnet $SrRuO_3$ *Phys. Rev. Lett.* **77** 2774

[22] Maeno Y, Hashingmoto H, Yoshida K, Ishizaki S, Fujita T, Bednorz J G and Lichtenberg F 1994 Superconductivity in a layered perovskite without copper *Nature* **372** 532

[23] Maeno Y, Rice T M and Sigrist M 2001 The intriguing superconductivity of strontium ruthenate *Phys. Today* **54** 42

[24] Cao G, McCall S, Shepard M, Crow J E and Guertin R P 1997 Magnetic and transport properties of single-crystal Ca_2RuO_4: relationship to superconducting Sr_2RuO_4 *Phys. Rev.* B **56** R2916

[25] Alexander C S, Cao G, Dobrosavljevic V, Lochner E, McCall S, Crow J E and Guertin P R 1999 Destruction of the Mott insulating ground state of Ca_2RuO_4 by a structural transition *Phys. Rev.* B **60** R8422

[26] Cao G, McCall S, Dobrosavljevic V, Alexander C S, Crow J E and Guertin R P 2000 Ground-state instability of the Mott insulator Ca_2RuO_4: impact of slight La doping on the metal–insulator transition and magnetic ordering *Phys. Rev.* B **61** R5053

[27] Puchkov A V, Schabel M C, N Basov D, Startseva T, Cao G, Timusk T and Shen Z-X 1998 Layered ruthenium oxides: from band metal to Mott insulator *Phys. Rev. Lett.* **81** 2747

[28] Ikeda S-I, Maeno Y, Nakatsuji S, Kosaka M and Uwatoko Y 2000 Ground state in $Sr_3Ru_2O_7$: Fermi liquid close to a ferromagnetic instability *Phys. Rev.* B **62** R6089

[29] Grigera S A *et al* 2001 Magnetic field-tuned quantum criticality in the metallic ruthenate $Sr_3Ru_2O_7$ *Science* **294** 329

[30] Crawford M K, Harlow R L, Marshall W, Li Z, Cao G, Lindstrom R L, Huang Q and Lynn J W 2002 Structure and magnetism of single crystal $Sr_4Ru_3O_{10}$: a ferromagnetic triple-layer ruthenate *Phys. Rev.* B **65** 214412

[31] Huang K Q, Soubeyroux J L, Chmaissem O, Natalisora I, Santoro A, Cava R J, Krajewski J J and Peck W F Jr 1994 Neutron powder diffraction study of the crystal structures of Sr_2RuO_4 and Sr_2IrO_4 at room temperature and at 10 *J. Solid State Chem.* **112** 355

[32] Cava R J, Batlogg B, Kiyono K, Takagi H, Krajewski J J, Peck W F Jr, Rupp L W and Chen C H 1994 Localized-to-itinerant electron transition in $Sr_2Ir_{1-x}Ru_xO_4$ *Phys. Rev.* B **49** 11890

[33] Crawford M K, Subramanian M A, Harlow R L, Fernandez-Baca J A, Wang Z R and Johnston D C 1994 Structural and magnetic studies of Sr_2IrO_4 *Phys. Rev.* B **49** 9198

[34] Cao G, Bolivar J, McCall S, Crow J E and Guertin R P 1998 Weak ferromagnetism, metal-to-nonmetal transition, and negative differential resistivity in single-crystal Sr_2IrO_4 *Phys. Rev.* B **57** R11039

[35] Cao G, Xin Y, Alexander C S, Crow J E, Schlottmann P, Crawford M K, Harlow R L and Marshall W 2002 Anomalous magnetic and transport behavior in the magnetic insulator $Sr_3Ir_2O_7$ *Phys. Rev.* B **66** 214412

[36] Cao G, Crow J E, Guertin R P, Henning P F, Homes C C, Strongin M, Basov D N and Lochner E 2000 Charge density wave formation accompanying ferromagnetic ordering in quasi-one-dimensional $BaIrO_3$ *Solid State Commun.* **113** 657

[37] Kim B J *et al* 2008 Novel $J_{\rm eff} = 1/2$ Mott state induced by relativistic spin–orbit coupling in Sr_2IrO_4 *Phys. Rev. Lett.* **101** 076402

[38] Moon S J *et al* 2008 Dimensionality-controlled insulator-metal transition and correlated metallic state in 5d transition metal oxides $Sr_{n+1}Ir_nO_{3n+1}$ ($n = 1$, 2, and ∞) *Phys. Rev. Lett.* **101** 226402

[39] Kim B J, Ohsumi H, Komesu T, Sakai S, Morita T, Takagi H and Arima T 2009 Phase-sensitive observation of a spin-orbital Mott state in Sr_2IrO_4 *Science* **323** 1329

[40] Landau L D and Lifshitz E M 1977 *Quantum Mechanics* 3rd edn (Oxford: Pergamon)

[41] Shanavas K V, Popovic Z S and Satpathy S 2014 Theoretical model for Rashba spin–orbit interaction in d electrons *Phys. Rev.* B **90** 165108

[42] Liu G-Q, Antonov V N, Jepsen O and Andersen O K 2008 Coulomb-enhanced spin–orbit splitting: the missing piece in the Sr_2RhO_4 puzzle *Phys. Rev. Lett.* **101** 026408

[43] Itoh M, Yoshiyuki Inaguma T S and Morii Y 1995 Structure of two-dimensional conductor of Sr_2RhO_4 *J. Solid State Chem.* **118** 206

[44] Martins C, Aichhorn M, Vaugier L and Biermann S 2011 Reduced effective spin-orbital degeneracy and spin-orbital ordering in paramagnetic transition-metal oxides: Sr_2IrO_4 versus Sr_2RhO_4 *Phys. Rev. Lett.* **107** 266404

[45] Qi T F, Korneta O B, Li L, Butrouna K, Cao V S, Wan X, Kaul R and Cao G 2012 Spin–orbit tuned metal–insulator transitions in single-crystal $Sr_2Ir_{1-x}Rh_xO_4$ ($0 \leqslant x \leqslant 1$) *Phys. Rev.* B **86** 125105

[46] Haverkort M W, Elfimov I S, Tjeng L H, Sawatzky G A and Damascelli A 2008 Strong spin–orbit coupling effects on the Fermi surface of Sr_2RuO_4 and Sr_2RhO_4 *Phys. Rev. Lett.* **101** 026406

[47] Wang F and Senthil T 2011 Twisted Hubbard model for Sr_2IrO_4: magnetism and possible high temperature superconductivity *Phys. Rev. Lett.* **106** 136402

[48] Lindquist A W and Kee H-Y 2019 Odd-parity superconductivity driven by octahedra rotations in iridium oxides (arXiv:1906.02749v1)

[49] Chen C *et al* 2020 Persistent insulating state at megabar pressures in strongly spin–orbit-coupled Sr_2IrO_4 *Phys. Rev.* B **101** 144102

[50] Cao G, Zhao H, Hu B, Pellatz N, Reznik D, Schlottmann P and Kimchi I 2020 Quest for new quantum states via field-editing technology (arXiv:2005.04327)

[51] Guertin R P, Bolivar J, Cao G, McCall S and Crow J E 1998 Negative differential resistivity in $Ca_3Ru_2O_7$: unusual transport and magnetic coupling in a near-metallic system *Solid State Commun.* **107** 263

[52] Higman T K, Miller L M, Favaro M E, Emanuel M A, Hess K and Coleman J J 1988 Room-temperature switching and negative differential resistance in the heterostructure hot-electron diode *Appl. Phys. Lett.* **53** 1623

[53] Jeong D S, Thomas R, Katiyar R S, Scott J F, Kohlstedt H, Petraru A and Hwang C S 2012 Emerging memories: resistive switching mechanisms and current status *Rep. Prog. Phys.* **75** 076502

[54] Chudnovskii F A, Pergament A L, Stefanovich G B, Somasundaram P and Honig J M 1997 Electronic switching in $CuIr_2S_{4-x}Se_x$ *Phys. Status Solidi* a **162** 601

[55] Pergament A L, Stefanovich G, Velichko A and Khanin S D 2006 Electronic switching and metal–insulator transitions in compounds of transition metals *Condensed Matter at the Leading Edge,* ed M P Das (New York: Nova Science Publishers) ch 1, pp 1–67

[56] Chudnovskii F A, Odynets L L, Pergament A L and Stefanovich G B 1996 Electroforming and switching in oxides of transition metals: the role of metal–insulator transition in the switching mechanism *J. Solid State Chem.* **122** 95

[57] Tsen A W *et al* 2015 Structure and control of charge density waves in two-dimensional 1T-TaS_2 *Proc. Natl Acad. Sci.* **112** 15054

[58] Okimura K, Ezreena N, Sasakawa Y and Sakai J 2009 Electric-field-induced multistep resistance switching in planar VO_2/c-Al_2O_3 structure *Jpn. J. Appl. Phys.* **48** 065003

[59] Okazaki R, Nishina Y, Yasui Y, Nakamura F, Suzuki T and Terasaki I 2013 Current-induced gap suppression in the Mott insulator Ca_2RuO_4 *J. Phys. Soc. Japan* **82** 103702

[60] Fujiyama S, Ohsumi H, Komesu T, Matsuno J, Kim B J, Takata M, Arima T and Takagi H 2012 Two-dimensional Heisenberg behavior of $J_{\rm eff} = 1/2$ isospins in the paramagnetic state of the spin-orbital Mott insulator Sr_2IrO_4 *Phys. Rev. Lett.* **108** 247212

[61] Dai J X, Calleja E, Cao G and McElroy K 2014 Local density of states study of a spin–orbit-coupling induced Mott insulator Sr_2IrO_4 *Phys. Rev.* B **90** 041102

[62] Ye F, Chi S X, Chakoumakos B C, Fernandez-Baca J A, Qi T F and Cao G 2013 Magnetic and crystal structures of Sr_2IrO_4: a neutron diffraction study *Phys. Rev.* B **87** 140406

[63] Boseggia S *et al* 2013 Locking of iridium magnetic moments to the correlated rotation of oxygen octahedra in Sr_2IrO_4 revealed by x-ray resonant scattering *J. Phys.: Condens. Matter* **25** 422202

[64] Torchinsky D H, Chu H, Zhao L, Perkins N B, Sizyuk Y, Qi T, Cao G and Hsieh D 2015 Structural distortion-induced magnetoelastic locking in Sr_2IrO_4 revealed through nonlinear optical harmonic generation *Phys. Rev. Lett.* **114** 096404

[65] Lobanov M V, Greenblatt M, Caspi E N, Jorgensen J D, Sheptyakov D V, Toby B H, Botez C E and Stephens P W 2004 Crystal and magnetic structure of the $Ca_3Mn_2O_7$ Ruddlesden–Popper phase: neutron and synchrotron x-ray diffraction study *J. Phys.: Condens. Matter* **16** 5339

[66] Jackeli G and Khaliullin G 2009 Mott insulators in the strong spin–orbit coupling limit: from Heisenberg to a quantum compass and Kitaev models *Phys. Rev. Lett.* **102** 017205

[67] Moon S J, Jin H, Choi W S, Lee J S, Seo S S A, Yu J, Cao G, Noh T W and Lee Y S 2009 Temperature dependence of the electronic structure of the $J_{\rm eff} = 1/2$ Mott insulator Sr_2IrO_4 studied by optical spectroscopy *Phys. Rev.* B **80** 195110

[68] Korneta O B, Qi T F, Chikara S, Parkin S, De Long L E, Schlottmann P and Cao G 2010 Electron-doped $Sr_2IrO_{4-\delta}$ ($0 \leqslant \delta \leqslant 0.04$): evolution of a disordered $J_{\rm eff} = 1/2$ Mott insulator into an exotic metallic state *Phys. Rev.* B **82** 115117

[69] Wang J C *et al* 2015 Decoupling of the antiferromagnetic and insulating states in Tb-doped Sr_2IrO_4 *Phys. Rev.* B **92** 214411

[70] Qi T F, Korneta O B, Parkin S, DeLong L E, Schlottmann P and Cao G 2010 Negative volume thermal expansion via orbital and magnetic orders in single-crystal $Ca_2Ru_{1-x}Cr_xO_4$ *Phys. Rev. Lett.* **105** 177203

[71] Chikara S, Korneta O, Crummett W P, DeLong L E, Schlottmann P and Cao G 2009 Giant magnetoelectric effect in the $J_{\rm eff} = 1/2$ Mott insulator Sr_2IrO_4 *Phys. Rev.* B **80** 140407

[72] Franke I, Baker P J, Blundell S J, Lancaster T, Hayes W, Pratt F L and Cao G 2011 Measurement of the internal magnetic field in the correlated iridates Ca_4IrO_6, $Ca_5Ir_3O_{12}$, $Sr_3Ir_2O_7$ and Sr_2IrO_4 *Phys. Rev.* B **83** 094416

[73] Nakatsuji S, Ikeda S and Maeno Y 1997 Ca_2RuO_4: new Mott insulators of layered ruthenate *J. Phys. Soc. Japan* **66** 1868–71

[74] Braden M, André G, Nakatsuji S and Maeno Y 1998 Crystal and magnetic structure of Ca_2RuO_4: magnetoelastic coupling and the metal–insulator transition *Phys. Rev.* B **58** 847–61

[75] Steffens P *et al* 2005 High-pressure diffraction studies on Ca_2RuO_4 *Phys. Rev.* B **72** 094104

[76] Terakura K and Fang Z 2001 Magnetic phase diagram of $Ca_{2-x}Sr_xRuO_4$ governed by structural distortions *Phys. Rev.* B **64** 020509

[77] Hotta T and Dagotto E 2001 Prediction of orbital ordering in single-layered ruthenates *Phys. Rev. Lett.* **88** 017201

[78] Lee J S, Lee Y S, Noh T W, Oh S-J, Yu J, Nakatsuji S, Fukazawa H and Maeno Y 2002 Electron and orbital correlations in $Ca_{2-x}Sr_xRuO_4$ probed by optical spectroscopy *Phys. Rev. Lett.* **89** 257402

[79] Jung J H, Fang Z, He J P, Kaneko Y, Okimoto Y and Tokura Y 2003 Change of electronic structure in Ca_2RuO_4 induced by orbital ordering *Phys. Rev. Lett.* **91** 056403

[80] Gorelov E, Karolak M, Wehling T O, Lechermann F, Lichtenstein A I and Pavarini E 2010 Nature of the Mott transition in Ca_2RuO_4 *Phys. Rev. Lett.* **104** 226401

[81] Liu G-Q 2011 Spin–orbit coupling induced Mott transition in $Ca_{2-x}Sr_xRuO_4$ ($0 \leqslant x \leqslant 0.2$) *Phys. Rev.* B **84** 235136

[82] Nakamura F *et al* 2002 From Mott insulator to ferromagnetic metal: a pressure study of Ca_2RuO_4 *Phys. Rev.* B **65** 220402

[83] Zegkinoglou I *et al* 2005 Orbital ordering transition in Ca_2RuO_4 observed with resonant x-ray diffraction *Phys. Rev. Lett.* **95** 136401

[84] Nakatsuji S and Maeno Y 2000 Quasi-two-dimensional Mott transition system $Ca_{2-x}Sr_xRuO_4$ *Phys. Rev. Lett.* **84** 2666–9

[85] Snow C S, Cooper S L, Cao G, Crow J E, Fukazawa H, Nakatsuji S and Maeno Y 2002 Pressure-tuned collapse of the Mott-like state in $Ca_{n+1}Ru_nO_{3n+1}$ ($n = 1,2$): Raman spectroscopic studies *Phys. Rev. Lett.* **89** 226401

[86] Qi T F, Korneta O B, Parkin S, Hu J and Cao G 2012 Magnetic and orbital orders coupled to negative thermal expansion in Mott insulators $Ca_2Ru_{1-x}M_xO_4$ (M = Mn and Fe) *Phys. Rev.* B **85** 165143

[87] Hu B, Zhao H, Answarthan S and Cao G 2019 unpublished

[88] Lovesey S W, Khalyavin D D, Manuel P, Chapon L C, Cao G and Qi T F 2012 Magnetic symmetries in neutron and resonant x-ray Bragg diffraction patterns of four iridium oxides *J. Phys.: Condens. Matter* **24** 496003

[89] Kim J W, Choi Y, Kim J, Mitchell J F, Jackeli G, Daghofer M, van den Brink J, Khaliullin G and Kim B J 2012 Dimensionality driven spin-flop transition in layered iridates *Phys. Rev. Lett.* **109** 037204

[90] Mattoni G, Yonezawa S and Maeno Y 2020 Diamagnetic-like response from localised heating of a paramagnetic material (arXiv:2004.04570)

[91] Sow C, Yonezawa S, Kitamura S, Oka T, Kuroki K, Nakamura F and Maeno Y 2017 Current-induced strong diamagnetism in the Mott insulator Ca_2RuO_4 *Science* **358** 1084–7

Sow C, Yonezawa S, Kitamura S, Oka T, Kuroki K, Nakamura F and Maeno Y 2020 Retraction *Science* **368** 376

[92] Sow C, Numasaki R, Mattoni G, Yonezawa S, Kikugawa N, Uji S and Maeno Y 2019 *In situ* control of diamagnetism by electric current in $Ca_3(Ru_{1-x}Ti_x)_2O_7$ *Phys. Rev. Lett.* **122** 196602

Sow C, Numasaki R, Mattoni G, Yonezawa S, Kikugawa N, Uji S and Maeno Y 2019 Retraction: *in situ* control of diamagnetism by electric current in $Ca_3(Ru_{1-x}Ti_x)_2O_7$ *Phys. Rev. Lett.* **124** 169902